The increase in cell volume and nuclear number of the koji-fungus *Aspergillus oryzae* contributes to its high enzyme productivity

Ayaka Itani[1], Haruto Motomura[1], Ken Oda[2], Hideyuki Yamashita[3], Kanae Sakai[4], Ken-ichi Kusumoto[4], Shinsuke Shigeto[5], Takehiko Ichikawa[6], Hosain Mohammad Mubarak[6], Takeshi Fukuma[6], Takuya Katayama[7,8], Jun-ichi Maruyama[7,8], Shunsuke Masuo[1], Naoki Takaya[1], Norio Takeshita[1*]

[1] Microbiology Research Center for Sustainability (MiCS), Faculty of Life and Environmental Sciences, Tsukuba Institute for Advanced Research (TIAR), University of Tsukuba, Tsukuba, 305-8572, Japan

[2] National Research Institute of Brewing, 3-7-1 Kagamiyama, Higashi-hiroshima, Hiroshima, 739-0046, Japan

[3] Higuchi Matsunosuke Shoten Co., Ltd., 1-14-2 Harima-cho, Abeno-ku, Osaka 545-0022, Japan

[4] Department of Biotechnology, Graduate School of Engineering, Osaka University, 2-1 Yamadaoka, Suita, Osaka 565-0871, Japan

[5] Department of Chemistry, School of Science, Kwansei Gakuin University, Sanda, Hyogo, 669-1330, Japan

[6] Nano Life Science Institute (WPI-NanoLSI), Kanazawa University, Kakuma-machi, Kanazawa 920-1192, Japan

[7] Department of Biotechnology, The University of Tokyo, Tokyo 113-8657, Japan

[8] Collaborative Research Institute for Innovative Microbiology, The University of Tokyo, Tokyo 113-8657, Japan

* Correspondence to: Norio Takeshita, takeshita.norio.gf@u.tsukuba.ac.jp

Abstract

While the ratio of nuclei to cell volume is well regulated, it remains largely unexplored in multinucleate organisms. The koji-fungus *Aspergillus oryzae*, traditionally used in Japanese brewing and fermentation for over a thousand years, is now widely utilized in modern biotechnology as a host for enzyme production. We discovered that, over time in culture, hyphae become thicker, resulting in a tenfold increase in cell volume, and the number of nuclei in hyphal cells also increases tenfold, exceeding 200. The increase in cell volume and nuclear number is unique among the investigated *Aspergillus* species and correlates with its high enzyme production capabilities. Since nuclear number and cell volume are correlated, both must increase simultaneously. Our analyses identified genetic factors involved in each of these increases. Increases in nuclear number and cell volume were also observed in other fungi bred for industrial use. This study not only deepens our understanding of the evolutionary processes that promote high enzyme productivity through fungal breeding, but also provides insights into the molecular mechanisms regulating cell volume and nuclear number in multinucleate organisms.

41 **Introduction**

42 In unicellular organisms, cell volume is tightly regulated in coordination with nuclear division timing
43 (1-3). Similarly, in multinucleated filamentous fungi, a correlation exists between cell volume and
44 nuclear number (4, 5). However, the number of nuclei varies across species (6), the factors governing
45 nuclear number and cell volume remain largely unknown. Filamentous fungi are industrially
46 significant microorganisms, and the strains selected through breeding provide ideal research models
47 for studying these evolutionary processes.

48 Filamentous fungi secrete a variety of hydrolytic enzymes to support their growth, and
49 humans have long harnessed this enzyme secretion ability for the production of a wide range of
50 fermented foods and beverages (7). *Aspergillus oryzae* has been used in Japan for over a thousand
51 years to produce traditional fermented foods like sake, soy sauce, and miso (8, 9). A distinctive feature
52 of the fermentation techniques is solid-state cultivation using substrates like rice, soybeans, and wheat
53 bran. The inoculum of *A. oryzae* used in fermentation, known as "koji," has been commercially
54 produced for around 700 years (10). Koji is created by cultivating koji-fungus on grains, and koji
55 starter manufacturers have selected and bred strains to improve the flavor and color of various
56 fermented products. The *A. oryzae* strains currently in use are mainly preserved and managed by koji
57 manufacturers and research institutions. A notable characteristic of *A. oryzae* is its high ability to
58 secrete starch-degrading enzymes and proteases, which has led to extensive research into its genome
59 and gene expression regulation (11-17).

60 Although *A. oryzae* shares 99.5% genomic similarity with *Aspergillus flavus*, which
61 produces the carcinogenic aflatoxin (18), there have been no reports of *A. oryzae* producing aflatoxins,
62 and its safety has been confirmed at the molecular level (19, 20). Phylogenomic analyses suggest that
63 *A. oryzae* and *A. flavus* diverged approximately 50,000 to 189,000 years ago (21, 22). Over the
64 following millennia, human use of *A. oryzae* is thought to have driven significant genomic

65 recombination, resulting in its evolution into a "cell factory" specifically optimized for the breakdown
66 of sugars and proteins (23).

67 Additionally, modern biotechnology utilizes filamentous fungi as cell factories to produce
68 organic acids, enzymes, and pharmaceuticals (24-26). *A. oryzae* also shows high production capacity
69 as a host for both homologous and heterologous protein production in modern biotechnology (27, 28).
70 Recently, its application has expanded to include the production of pharmaceutical proteins and
71 secondary metabolites (29, 30). Furthermore, filamentous fungi involved in fermentation play a crucial
72 role in creating a more sustainable food system, such as by upcycling agricultural by-products into
73 food through fungal fermentation and using *A. oryzae* mycelium for alternative meats (31, 32).

74 While basic and applied research on *A. oryzae* continues, fundamental questions remain
75 unanswered, such as why *A. oryzae* exhibits high enzyme production capacity and why it excels as a
76 host for heterologous expression. This study shows that the key lies in the increase in cell volume and
77 nuclear number, and analyzes the molecular mechanisms.

78

79 **Result**

80 **Increase in nuclear number and cell volume in *Aspergillus oryzae***

81 In the model strain *A. oryzae* RIB40, hyphae on day 1 of cultivation contain 10-20 nuclei per cell, but
82 by day 2 of cultivation, apical cells with more than 200 nuclei appear (33). We classified the hyphae
83 into three categories based on the number and distribution of nuclei, and compared their proportions
84 after 1 to 3 days of cultivation (see methods, images were shown previously)(33). We found that the
85 proportion of hyphae with a higher number of nuclei (represented by class III, over 200 nuclei in the
86 cell) increased as the culture period increased from 1 to 3 days (Fig. 1A, B) (33). This phenotype was
87 not observed in the model fungus *Aspergillus nidulans* or the closely related species *A. flavus* (Fig.
88 1A, B) (33). As far as we know, such phenotypes have not been observed in other strains of *Aspergillus*

89 *nidulans*, *Aspergillus niger*, *Aspergillus fumigatus*, or other strains commonly used in research.
90 Among other *Aspergillus* species used in fermentation (9, 10), the proportion of hyphae with a higher
91 number of nuclei increased in *Aspergillus sojae*, which is used for miso and soy sauce production.
92 This phenotype was not observed in *Aspergillus luchuensis* nor in its albino mutant *Aspergillus*
93 *luchuensis mut. kawachii*, which are used for distilled spirits such as awamori and shochu. Among
94 several strains of *A. oryzae* used in industrial applications, the RIB915 strain used for soy sauce
95 fermentation does not show an increase in the number of nuclei, while the RIB128 and RIB430 strains
96 used in sake brewing exhibit a significant increase in the number of nuclei, suggesting that different
97 phenotypes were selected through distinct breeding processes.

98 The distribution of nuclei in the hyphae of *A. oryzae* RIB40 was visualized through 3D
99 reconstruction (Fig. 1C, Movie 1). In the class I hyphae, the nuclei were spaced relatively evenly,
100 whereas in the class III hyphae with increased nuclei, the nuclei were densely packed and arranged in
101 a disordered manner. Furthermore, the nuclear size in the class III hyphae was significantly smaller
102 than that in the class I hyphae (Fig. 1D, E). Nuclear division is synchronized in the hypha even when
103 there are more than 200 nuclei (33), suggesting that DNA replication occurs similarly in most nuclei.
104 The germination rate of conidia and the colonies formed from individual conidia show no significant
105 abnormalities, suggesting, that nearly all nuclei possess normal genomes and chromosomes.

106 Strains without an increase in nuclear number had hyphae with diameters ranging from 2 to
107 7 μm, while strains with an increase in nuclear number had some hyphae of similar thickness but often
108 exhibited thicker hyphae exceeding 10 μm (Fig. 1F). We compared the number of nuclei and cell
109 volume within the first 100 μm from the hyphal tip, due to variation in the distance from the hyphal
110 tip to the septum, among *A. oryzae* strains (RIB40, RIB128, RIB915) and *A. flavus* (Fig. 1G). A strong
111 positive correlation was observed between number of nuclei and cell volume. This is consistent with
112 previously reports that the number of nuclei per hyphal volume remains constant (4, 5).

113

114 **Thick hyphae with increased nuclei emerge by branching**

115 Time-lapse imaging using the *A. oryzae* RIB40 expressing H2B-GFP indicated that thick hyphae with
116 increased nuclei emerged by branching from hyphae without increased nuclei (Fig. 2A, Movie 2). In
117 the emerged thick hyphae, rapid nuclear division occurred at the sites of branching (Fig. 2B, Movie
118 3). Immediately after branching, the thick hyphae showed a significantly faster rate of nuclear
119 proliferation, increasing 4–5 times within 8 hours compared to the thin hyphae immediately after
120 branching (Fig. 2C). In some cases, thick hyphae emerged by branching from thick hyphae (Fig. 2D,
121 left), while in other cases, thin hyphae emerged from thick hyphae (Fig. 2D, right).

122 Time-lapse imaging was conducted over a wider area, and image processing was applied to
123 color-code the nuclei: green for those in hyphae with increased nuclei and white for those in hyphae
124 without increased nuclei (Fig. 2E, Movie 4, Fig.S1A, see methods). Up to 24 hours after inoculation,
125 most hyphae were thin with no increase in nuclei number, but thick hyphae with increased nuclei
126 began to appear as time progressed (Fig. 2E, F). Since thick hyphae elongated faster than thin hyphae
127 (Fig. 2G), thick hyphae outgrew and overtook thin hyphae, eventually dominating the colony
128 perimeter (Fig. 2E, F).

129 Transmission electron microscopy confirmed basic nuclear structures, such as the nuclear
130 membrane and nucleolus, in both thick and thin hyphae (Fig. S1B). As hyphal diameter increased, cell
131 walls became more uneven and thicker (Fig. 2H, I). This finding corresponds with Raman
132 spectroscopy results showing pronounced peaks corresponding to cell wall polysaccharides in thick
133 hyphae (Fig. S1C)(34). Additionally, peaks associated with active mitochondria were prominent in
134 thick hyphae (Fig. S1C)(35), which was further confirmed by fluorescence staining (Fig. S1D). The
135 surface structure and mechanical properties of the cell wall were analyzed using atomic force
136 microscopy. Thick hyphae exhibited greater surface roughness and higher elasticity compared to thin

137 hyphae (Fig. 2J, K, Fig. S1E, F).

138

139 **Increase in nuclear number and enzyme secretion**

140 We compared the amounts of secreted proteins in *A. oryzae* RIB40, RIB128, RIB915, *A. nidulans*, and
141 *A. flavus* (Fig. 3A). The strains that show an increase in nuclear number had significantly higher levels
142 of protein secretion than the strains that do not. In this condition, α-amylases are the dominant proteins
143 secreted by *A. oryzae* (15). The amylase enzyme activity was compared between in *A. oryzae* RIB40,
144 which shows an increase in nuclear number, and *A. oryzae* RIB915, which does not show an increase.
145 In RIB40, starting from day 2, when hyphae with increased nuclear numbers appeared, the enzyme
146 activity per fungal biomass significantly increased more than RIB915 (Fig. 3B).

147 To compare the amylase activity between hyphae with a higher and a lower number of nuclei,
148 amylase activity was monitored under conditions where a single hypha grew in a microfluidic channel
149 with a fluorescent substrate (Fig. 3C, S2A, Movie 5)(36). After 12 hours, the fluorescence intensity in
150 the channel with thick hyphae was about three times higher than that in the channel with thin hyphae,
151 indicating that thicker hyphae secreted more amylase than thinner hyphae (Fig. 3D).

152 We found that addition of yeast extract increased in both hyphal width and nuclear number
153 in the RIB915 strain (Fig. 3E, Fig. S2B). In *A. oryzae* RIB40, the addition of yeast extract did not
154 make the already thick hyphae any thicker but increased the proportion of thicker hyphae. Addition of
155 yeast extract increased protein secretion approximately 1.8 times in RIB40 and 8.5 times in RIB915
156 (Fig. 3F). Althouth the addition of yeast extract did not cause a dramatic increase in nuclear number
157 in *A. nidulans*, hyphal width increased by 1.4-times and protein secretion increased by 5.1-times.

158 The addition of nucleic acids, peptone, or casamino acids to the minimal medium increased
159 the number of nuclei in *A. oryzae* RIB915, while vitamin B did not cause a significant change in
160 nuclear number (Fig. S2C). Although the addition of individual amino acids did not show the same

161 effect as yeast extract, the addition of asparagine, proline, glutamine, and branched-chain amino acids
162 increased the proportion of hyphae with increased nuclei by 40-50% (Fig. 3G, Fig. S2D). The amino
163 acids that induced nuclear number increase also led to an increase in protein secretion, indicating a
164 positive correlation between the ratio of class III hyphae and the increase in secreted proteins (Fig. 3H,
165 Fig. S2E). Since the amino acids inducing an increase in nuclear number may activate the TOR
166 pathway (37), *A. oryzae* RIB40 was grown with low concentration of rapamycin, a TOR pathway
167 inhibitor, which minimally affects colony size. Under the conditions, RIB40 did not produce hyphae
168 with an increased number of nuclei (Fig. 3I-K, Fig. S2F). Rapamycin decreased the ratio of hyphae
169 with increased nuclei even in the medium with yeast extract (Fig. S2G).
170
171 **Transcriptome analyses in hyphae with increased nuclei**
172 To investigate gene expression changes in hyphae with increased nuclei, transcriptome analysis was
173 performed under six conditions: In minimal medium; *A. oryzae* RIB40, which shows increased nuclei,
174 *A. oryzae* RIB915 and *A. nidulans*, which do not show increased nuclei. In minimal medium with yeast
175 extract, *A. oryzae* RIB40 and RIB915, which shows increased nuclei, and *A. nidulans,* which do not
176 show increased nuclei (Fig. 4A, Fig. S2B). In RIB915, supplementation with yeast extract led to a
177 more than four-fold increase in the expression of 660 genes, among which 449 genes did not show
178 such increase in RIB40 or *A. nidulans* (Fig. 4B, Table S1). GO analysis of these genes revealed that
179 process related to cell wall synthesis and divalent metal ion transport were significantly enriched (Fig.
180 4C).
181 To capture gene expression changes associated with increased nuclei with higher resolution,
182 thick and thin hyphae from RIB40 were dissected using laser microdissection, collected separately,
183 and subjected to transcriptome analysis (Fig. 4D, Movie 6). Clear differences in gene expression
184 pattern were observed between thick and thin hyphae (Fig. 4E). 558 genes that were more than four-

185 fold upregulated in thick hyphae but not in thin hyphae (Table S2). GO analysis of the upregulated
186 genes indicated an enrichment of processes related to biogenesis of ribosome and cellular component
187 (Fig. 4F). Among them, 21 matched those from Table S1 (Fig. 4G, Table S3). Of these, 13 had GO
188 annotations, which were related to conidiation, cell wall synthesis, Ca^{2+} transport and rRNA
189 processing (Fig. 3H). KEGG map visualization indicates that overall ribosomal gene expression
190 increased in the thick hyphae than the thin hyphae (Fig. S3A).

191 Among the gene list, we focused on *msy1* and *msy2*, which are involved in Ca^{2+} transport
192 and maintaining cell volume homeostasis in *Schizosaccharomyces pombe* (38, 39). Disruption of the
193 orthologue genes, *msyA* and *msyB,* in *A. oryzae* RIB40 did not have a significant impact on colony
194 growth, hyphal morphology and number of nuclei in minimal medium (Fig. S3B). Under hypoosmotic
195 shock conditions, the Δ*msyA* often indicated cell lysis near the hyphal tips (Fig. 4I, J). Under
196 hypoosmotic conditions, water influx into the cells causes hyphal cell expansion, but the volume and
197 turgor pressure are regulated to prevent cell lysis. The *msyA* disruption, however, impairs the
198 regulation of the hyphal cell expansion, leading to hyphal lysis (Fig. S3C-E).

199

200 **SNP analysis among industrial strains with distinct phenotypes**

201 The fact that currently used *A. oryzae* strains are managed and preserved by koji manufacturers and
202 research institutions is a notable advantage of *A. oryzae* research. Whole-genome sequencing and
203 comparative genome analysis of 82 *A. oryzae* strains with different applications have shown that these
204 strains cluster into several clades (24). We investigated whether nuclear numbers increase in 20 strains
205 selected from six different clades (Fig. 5A). In the minimal media supplemented with yeast extract, all
206 strains exhibited an increase in nuclear number (Fig. S4A). In the minimal media without yeast extract,
207 three strains from Clade C showed an increase in nuclear number, whereas strains from Clades A, B,
208 and E did not (Fig. 5A, B, Fig. S4A). Clades F and G included both strains with increased nuclear

209 numbers and strains without. SNP analysis of ORFs in Clades F and G revealed 108 mutations in
210 Clade F between TK-32 and TK-38, and 23 mutations in Clade G between TK-41 and TK-47 (Table
211 S4 and S5).

212 Among these, AO090038000626; *rseA*, predicted glycosyl transferase, was the only
213 common gene. This gene has been identified as a mutation in a *A. sojae* mutant with high extracellular
214 enzyme production (40). It is also shown that deletion of *rseA* in *A. nidulans* leads to cell wall defects
215 and promotes enzyme secretion (40). Comparison of mutations in *rseA* among strains in Clade C, F
216 and G indicates a few amino acid substitutions within the ORF, but no common mutations
217 corresponded to the phenotype (Fig. 5C, Fig. S4B). Structural prediction suggests that the mutations
218 are located inside the enzyme domain (Fig. S4C).

219 The disruption of the *rseA* in *A. oryzae* RIB40 resulted in significant growth delay, increased
220 branching, and the absence of hyphae with increased nuclei (Fig. 5D, Fig. S4D). The *rseA* gene DNA
221 fragments from the strains with increased nuclei (RIB40, TK-47) or from the strain without increased
222 nuclei (TK-41) were amplified by PCR and introduced ectopically into RIB915 (Fig. 5E). The strains
223 expressing *rseA* from RIB40 or TK-47 exhibited an increase in hyphal width and a corresponding
224 increase in the proportion of hyphae with more nuclei, whereas the strain expressing *rseA* from TK41
225 showed no increase in hyphal width or nuclear number (Fig. 5E, F, Fig. S4E).

226

227 **Industrial breeding strains from other genera**

228 To investigate whether the phenomenon of increased nuclear numbers also applies to other industrial
229 fungi, we compared the bred strain of *Trichoderma reesei* (QM9414) for cellulase production and its
230 control strain (QM6a)(41), as well as the bred strain of *Penicillium chrysogenum* (IFO4688) for
231 penicillin production and wild type strain (42). In minimal medium, no significant differences in
232 hyphal width or nuclear number were observed between the bred and control strains, whereas with the

233 addition of yeast extract, a notable increase in nuclear number and hyphal width was observed only in
234 the bred strains (Fig. 5G, H, Fig. S5A-C). The addition of yeast extract significantly increased cellulase
235 and protease activity only in the bred strain of *T. reesei* and *P. chrysogenum,* respectively (Fig. 5I, J).
236 These results suggest that even in modern biotechnology, where high enzyme or compound producing
237 strains are bred, strains with increased nuclear numbers were selected, like the traditional breeding
238 practices of koji-fungi.
239

240 **Discussion**

241 In *A. oryzae* some strains, hyphae grow about three times thicker and contain roughly ten times more
242 nuclei than the initial hyphae (Fig. 1). These thicker hyphae emerge from existing branches, where
243 nuclear division is promoted, resulting in the formation of hyphae with an increased number of nuclei
244 (Fig. 2). A clear correlation was observed between hyphal cell volume and nuclear number (Fig. 1G).
245 This consistency aligns with findings in other organisms, from unicellular yeast to multicellular plants
246 and animals, where the nuclear-to-cytoplasmic ratio is tightly regulated, allowing cell cycle
247 progression only upon reaching a critical cell size (1-3). Both the G1/S and G2/M transitions are
248 controled by size checkpoints, with specific mechanisms differing between species (44, 45).

249 In *A. nidulans*, it is known that the duration of the G1 and G2 phases is regulated by
250 temperature (46). While the mechanisms governing the G1/S phase transition remain unclear (47), the
251 G2/M phase transition has been shown to involve the following: During the interphase of *A. nidulans*,
252 NimX (CDK1) binds to NimE (cyclin B), and its activity is regulated through phosphorylation by
253 AnkA (Wee1 kinase) and NimT (Cdc25 phosphatase)(48-50). The activated NimX-NimE complex
254 subsequently dephosphorylates by NimT and activates NimA (Never-in-Mitosis A) protein kinase (51,
255 52). NimA is essential for the transition from G2 to mitosis, and its expression is tightly regulated
256 during the cell cycle (52). The mRNA level of *nimA* and *nimT* begin to increase in G2, reach a plateau

257 during late G2 and M phases, and are sharply degraded at the end of mitosis upon re-entry into
258 interphase (52, 53), meaning high expression levels of *nimA* and *nimT* result in a longer G2 phase. In
259 thick hyphae, *nimA* and *nimT* mRNA was hardly detected, suggesting that thick hyphae sense cell
260 volume in some way and subsequently shorten the G2 phase (Fig. 6A). The expression level of *nimE*
261 was low in both thick and thin hyphae, with no significant difference observed. As known in other
262 organisms, its function is likely regulated through phosphorylation and the protein degradation.

263 Branching is thought to occur through the degradation and reconstruction of the cell wall at
264 the branching site (54). SNP analysis between industrial strains with different phenotypes identified
265 RseA, a predicted glycosyltransferase (Fig. 5). Deletion of *rseA* caused defects in cell wall synthesis
266 in *A. nidulans*, leading to increased enzyme secretion (40, 55). Although the targets of RseA are
267 unknown, RseA could be involved in the cell wall integrity by modifying glycosyl chains on enzymes
268 responsible for cell wall synthesis and degradation. Mutations in *rseA* may impair the regulation of
269 cell wall loosening at the branching site, resulting in the formation of thicker hyphae. In fact, in the
270 thick hyphae of RIB40, localized imbalances in cell wall components have been demonstrated by TEM
271 and AFM.

272 Thicker hyphae can only form if high turgor pressure is maintained within the hyphae, in
273 addition to changes in cell wall remodeling during branching. *msyA* and *msyB*, whose orthologues are
274 calcium channels involved in the regulation of cell volume, were identified among the genes that show
275 a significant increase in expression in thicker hyphae (Fig. 4)(38, 39). Analysis of the knockout strains
276 demonstrated the function of cell volume regulation adapted to increased turgor pressure in
277 hypoosmotic conditions. The function of these calcium channels is likely crucial for maintaining the
278 balance of turgor pressure and cell volume.

279 The Target of Rapamycin (TOR) pathway is a central regulator of cellular growth,
280 responding to a variety of nutrients, such as amino acids, and carbon sources, as well as environmental

281 factors like oxygen levels, osmotic pressure, pH, and temperature stress (56, 57). Upon sensing these
282 inputs, the TOR pathway influences translation activity, metabolic flow, and cell size (57, 58). In both
283 yeast and mammalian models, amino acids like branched-chain amino acids (BCAAs), glutamine, and
284 alanine are crucial for nutrient sensing, forming the basis for TOR signaling activation (58-60). These
285 amino acids are like those contributing to nuclear increase in the RIB915 strain (Fig. 3G). Furthermore,
286 TOR inhibition by rapamycin in the RIB40 strain suppressed the formation of hyphae with increased
287 nuclei (Fig. 3I-K). Consistent with the activation of translation by the TOR pathway, the expression
288 of ribosome-related genes was elevated in thicker hyphae (Fig. S3A). The TOR pathway directly
289 regulates mitochondrial activity (61). Thick hyphae exhibited heightened mitochondrial density and
290 activity (Fig. S1C, D), suggesting that the TOR pathway support the high ATP demand associated with
291 rapid biosynthesis.

292 Cell volume and nuclear number mutually regulate each other, meaning that thicker hyphae
293 always possess more nuclei. For the formation of thicker hyphae with numerous nuclei, an increase in
294 cell volume and a corresponding increase in nuclei must occur simultaneously (Fig. 6A). In our model,
295 cell wall loosening at a branching site and regulation of cell volume by turgor pressure constitute
296 necessary conditions for increasing cell volume and maintaining thick hyphae. RseA and MsyA may
297 be involved in these processes. At the same time, enhanced translational capacity, possibly due to
298 increased expression of ribosomal genes associated with TOR activation, and mechanisms that
299 accelerate the cell cycle represent another essential condition that enables an increase in nuclear
300 number. Both genetic potential and nutritional environmental signals are likely required for the
301 formation of thick hyphae with a high number of nuclei. In the *A. oryzae* RIB915 strain, the number
302 of nuclei and cell volume increased in response to specific amino acids, whereas in the *A. oryzae*
303 RIB40 and other strains, both increased even without the addition of such amino acids, suggesting that
304 they possesses the genetic potential to respond independently of nutritional signals. When thick

305 hyphae were cultured on fresh medium, thin hyphae initially emerged, suggesting the necessity of
306 sustained high metabolic activity. Weakening the cell wall by treatment with a low concentration of
307 calcofluor white did not lead to hyphal thickening or an increase in nuclear number. On the contrary,
308 thick hyphae have thicker cell walls (Fig. 2H-K), which are necessary to maintain the increased cell
309 volume.

310 *A. nidulans* and *A. flavus* did not exhibit an increase in nuclear number. *A. sojae* displayed
311 increased nuclear numbers, whereas *A. kawachii* and *A. luchuensis* did not (Fig. 1). The 20 strains of
312 *A. oryzae* selected from different clades showed an increase in nuclear number in the minimal medium
313 supplemented with yeast extract. In the medium without yeast extract, there were strains that showed
314 an increase in nuclear number and others that did not. These differences might be due to variations in
315 their applications or the selection of strains with diverse characteristics, such as not only enzyme
316 activity but also their impact on the flavor, aroma, and color of the final products. Additionally, there
317 might be dominant mutations that activate TOR pathway even in the minimal medium. Multiple gene
318 mutations were identified as contributing to the phenotype of increased hyphal volume and nuclear
319 number, suggesting that the phenotype was not the result of a single mutation but rather the gradual
320 accumulation of mutations through breeding. The koji-fungus strains used to produce high-quality
321 sake and soy sauce have been selectively bred over many years, long before the advent of modern
322 biotechnology, to enhance their saccharolytic and proteolytic activities. Modern biotechnological bred
323 strains such as *T. reesei* QM9414 and *P. chrysogenum* IFO4688 also exhibit a phenotype of thicker
324 hyphae with increased nuclear numbers under nutrient-rich conditions (Fig. 5). This consistency
325 suggests that by breeding naturally multinucleate filamentous fungi under nutrient-rich conditions, it
326 is possible to obtain strains with increased nuclear numbers and enhanced enzyme or compound
327 production.

328 A previous study reported an increase in the number of nuclei in *A. nidulans* (62, 63). Here,

329 we examined the nuclear distribution of *A. nidulans* grown on the culture media, however, did not find
330 class III hyphae as observed in *A. oryzae*. Even in *A. nidulans*, conidiophore stalks contain a high
331 number of nuclei. It has been shown that *A. oryzae* has a taller conidiophore stalk (64). In the thick
332 hyphae of *A. oryzae*, the expression level of *flbA*, an early regulator of conidiophore development (65),
333 was elevated. This suggests that differentiation to aerial hyphae may be involved in the increase of
334 hyphal volume and nuclear number.

335 We investigated whether the reduction in nuclear size observed in thick hyphae was due to
336 a change from diploid to haploid status. However, no difference in GFP-histone fluorescence intensity
337 was detected between thick and thin hyphae (Fig. S5D). In both RIB40 and RIB915 strains, no
338 significant difference in conidial spore size was observed despite the large difference in the number of
339 nuclei within the hyphae (Fig. S5E). These results suggest that both thick and thin hyphae remain
340 haploid, and that the smaller nuclear size observed in thick hyphae is likely due to a higher nuclear
341 density.

342 The number of nuclei in filamentous fungi varies greatly among species (66). For example,
343 *Neurospora crassa* can exceed 100 nuclei, which correlates with its exceptionally rapid growth rate
344 and high protein secretion capacity (67). An increase in the number of nuclei per cell is expected to
345 enhance transcription and translation per cell, thereby improving enzyme production and secretion
346 capacity (Fig. 6B). Whereas, maintaining a high nuclear number requires a substantial amount of
347 energy, and in conditions where external nutrient supply is insufficient, cells rapidly die. Thus, the
348 tendency to maintain a high nuclear number could be a selective pressure unlikely to occur in nature.
349 The regulation of nuclear number and its ecological strategy are intriguing in other fungi such as *N.*
350 *crassa*, which rapidly spreads after wildfires (68), and arbuscular mycorrhiza fungi that form
351 symbiotic relationships with plants and contain thousands of nuclei within hyphae lacking septa (69).
352 In any case, koji-fungus strains were bred specifically for high enzyme production in nutrient-rich

353 environments, and we propose that some of them acquired the specialized trait of increased cell volume
354 and nuclear number through selection. This study elucidates the evolutionary processes driven by
355 breeding selection in *A. oryzae* and the underlying mechanisms contributing to high enzyme
356 productivity. These findings not only offer new approaches for optimizing filamentous fungi for
357 bioindustry applications but also lead to the elucidation of the molecular mechanisms regulating cell
358 volume and nuclear number in multinucleated organisms.
359
360
361
362
363
364 **Acknowledgements.**

365 This work was funded by MEXT KAKENHI grant number 21H02095, 21K19062, 25K01927 and
366 Scientific Research on Innovative Areas "Post-Koch Ecology" grant number 22H04878 to NT.
367 Ohsumi Frontier Science Foundation, Noda Institute for Scientific Research Grant, and Japan Science
368 and Technology Agency (JST) ERATO grant number JPMJER1502 to NT. AFM measurement was
369 supported by the World Premier International Research Center Initiative (WPI).

370

371 **Methods**

372 **Strains and Culture Conditions.** The filamentous fungal strains used in this study are listed in Table
373 S6. *A. oryzae* RIB40 expressing H2B-GFP, UtH2BG stain, is described previously (33). Minimal
374 medium for *Aspergillus* species was shown in Table S7. When peptone, casamino acids, or yeast
375 extract was added, the final concentration was 1%. Amino acids were added at a final concentration
376 of 0.1%, B vitamins (biotin, pyridoxine hydrochloride, thiamin hydrochloride, riboflavin, PABA, and
377 nicotinic acid) were added at 100 μM, and nucleotides (inosine and uridine) were added at 10 mM.
378 **Genetic Manipulation.** To delete target genes, genome editing plasmids and circular donor DNA
379 plasmids were constructed as described previously (70). The sgRNA cassette was designed under the
380 U6 promoter with the following target sequences: GTGACGATCTACGGTAACGC for the *msyA* gene,
381 GATCAGTTGAGCGTCCCCTA for the *msyB* gene, and AGCTAGCGCAGCCGGTCTGC for the
382 *rseA* gene. The genome editing plasmid was constructed by introducing the sgRNA expression cassette
383 into the SmaI restriction site of the pRGE-gRT6 plasmid (70). For the donor plasmid, 1 kb fragments

upstream and downstream of the target genes were amplified, ligated, and inserted into the linearized pUC19 vector (Takara Bio). Both plasmids were applied for transformation using the *A. oryzae* RIB40 strain. To amplify *rseA* region, spanning 1 kb upstream to 1 kb downstream, the templates used were *A. oryzae* RIB40, TK-42, and TK-47 strains. The amplified fragments were inserted into the HindIII site of the pPTRI vector (TaKaRa) to construct the plasmid. Transformations were performed using the protoplast-PEG method according to the manufacturer's protocol for pPTRI. Transformants were selected on the minimal medium plates containing 0.1 mg/l pyrithiamine. Integration of constructs was confirmed by PCR analysis.

Microscopy. Images were captured using an Axio Observer Z1 inverted epifluorescence microscope (Carl Zeiss) equipped with Plan-Apochromat objectives, an AxioCam 506 mono camera, and a Colibri.2 LED light source. The stage temperature was maintained at 30°C with a thermoplate (Tokai Hit). Nuclei were stained with SYBR Green (Takara), mitochondria with Rhodamine 123 (Invitrogen), the cell membrane with FM4-64 (Invitrogen). Images were collected using Zen (Carl Zeiss) and ImageJ software.

Image Analysis. The distribution pattern of nuclei was classified into the following three types; Class I: nuclei distribute at a constant interval without overlapping; Class II: nuclei align but sometimes overlap; Class III: nuclei scattered throughout hyphae but not aligned. Nuclei, hyphal size, and fluorescence intensity were quantified using Zen and ImageJ software. Z-stack 3D reconstruction and nuclear color coding were performed with Imaris (Oxford Instruments). Hyphal elongation distances were analyzed using the MTrackJ plugin in ImageJ. For Fig. 2E, nuclei were binarized, and those in non-increased hyphae were displayed in white based on size and circularity.

Transmission Electron Microscopy (TEM). The culture samples were embedded in 1% water agar and fixed with 2.5% glutaraldehyde in 0.1 M phosphate buffer (pH 7.0) at room temperature for 2 hours. Sample preparation and sectioning were performed at the Institute of Medicine, University of Tsukuba. Observations were conducted using a JEM-1400 transmission electron microscope (JEOL).

Imaging with Microfluidic Devices. Microfluidic devices were fabricated as described previously (33). Two types of devices were constructed: a 2D observation device to visualize hyphal expansion (Fig. S1A) and a single-hypha isolation device for enzymatic activity measurement (Fig. S2A). Conidia suspensions were loaded into a 10 ml plastic syringe (SS-10ESZ, Terumo) and connected to polyethylene tubing (inner diameter 0.38 mm, outer diameter 1.09 mm, BD Intramedic). Air was expelled from the syringe, and the suspension was injected into the device inlet. The number of conidia flowing through the microfluidic channel was adjusted under a microscope. The syringe was then replaced with another containing medium, and the medium was delivered at the minimum flow rate using a syringe pump (YSP-101, YMC). The device was incubated at 30°C on a thermal stage (TOKAI HIT) and imaged using an Axio Observer Z1 microscope (Carl Zeiss). α-amylase activity in the device was measured using the EnzChek Ultra amylase assay kit (Invitrogen).

420 **Enzyme Activity Assays.** Fungal conidia 10^4 were inoculated onto 25 ml of medium in a petri dish
421 and statically cultured at 30 ºC for 4 days. Protein concentration and enzymatic activities in the culture
422 supernatant were measured. Protein quantification was performed using the Bradford assay (Protein
423 Assay Kit, BIO-RAD), with bovine gamma globulin as the standard. Carboxymethyl cellulase
424 (CMCase) activity was determined by measuring reducing sugars using the 3,5-dinitrosalicylic acid
425 method. CMCase activity was assayed at 50 ºC for 15 min in a reaction mixture containing 50 mM
426 sodium acetate buffer (pH 5.0) and 1% carboxymethyl cellulose. One unit of enzyme activity was
427 defined as the amount of enzyme required to release 1 μmol of reducing sugar (as glucose equivalent)
428 per minute. α-amylase activity was measured using an α-Amylase Assay Kit (Kikkoman Biochemifa)
429 according to the manufacturer's instructions. Acid carboxypeptidase (ACP) activity was determined
430 using the Acid Carboxypeptidase Assay Kit (Kikkoman Biochemifa) following the provided protocol.
431 **RNA-seq Analysis.** Sterilized cellophane was placed on agar plates, and conidia were inoculated.
432 After culturing at 30 ºC for 3 days, samples were frozen, homogenized with a mortar and pestle, and
433 total RNA was extracted using the RNeasy Mini Kit (QIAGEN). Library preparation, sequencing, and
434 partial data analysis were performed by the Faculty of Medicine, University of Tsukuba. Sequencing
435 was conducted using 36 bp paired end reads on the Illumina NextSeq 500, and reads were mapped to
436 the *A. oryzae* RIB40 reference genome using the CLC Genomic Workbench (QIAGEN). For laser
437 microdissection, sterilized membrane slides (Carl Zeiss) were immersed in MM liquid, and conidia
438 were inoculated onto the membrane. After static culturing at 30 ºC for 3 days, sections were collected
439 using a PALM MicroBeam laser microdissection system (Carl Zeiss). RNA was extracted from 500-
440 700 sections respectively using the RNeasy Mini Kit. Library preparation and sequencing were
441 performed by Takara Bio Inc., using 150 bp paired end reads on the Illumina NovaSeq 6000. Reads
442 were mapped to the *A. oryzae* RIB40 reference genome using the CLC Genomic Workbench. Genes
443 showing a ≥4-fold change in expression were considered significant, and gene ontology (GO)
444 enrichment analysis of biological processes was performed using ShinyGO 0.81 (71). Heatmaps were
445 visualized using the Python Seaborn package (72). Gene annotations were obtained from FungiDB.
446 **Low Osmotic Pressure Shock Analysis.** Conidia were spot inoculated onto the minimal medium
447 containing 1 M NaCl and cultured at 30 ºC for 3 days. Colony tips were treated with distilled water
448 for 3 min, and the number of tip ruptures was counted. Hyphal tip swelling was assessed by staining
449 hyphae cultured in the minimal medium liquid for 3 days with FM4-64, mounting them on a coverslip
450 with a small volume of medium, and adding an equal volume of distilled water.
451 **Raman Spectroscopy.** The conidia were inoculated into minimal medium liquid in a glass-bottom
452 dish and cultured at 30 ºC for 3 days. Raman spectra were acquired using an XploRA PLUS Raman
453 microscope, as described previously (32). Hyphae attached to the dish bottom were irradiated with a
454 532 nm laser at 0.93 mW for 30 seconds. Spike artifacts caused by cosmic rays were manually removed.
455 Ten spectra were averaged, and background signals attributed to the medium and glass were subtracted.

Protein Structure Analysis. RseA protein structure was predicted using AlphaFold2 and visualized with PyMOL (v1.20). Domains were annotated using InterPro.

Atomic Force Microscopy (AFM). The conidia were inoculated into minimal medium liquid on a Poly-L-Lysine-coated (Sigma Aldrich) glass-bottom dish (ibidi) and cultured at 30 ºC for 3 days. We used a JPK Nanowizard 4 (Bruker) equipped with an inverted fluorescence microscope (Eclipse Ti2, Nikon). The temperature was maintained at 30 ºC using a dish heater integrated into the stage. BL-AC40TS-C2 cantilevers (Olympus, spring constant approximately 0.1 N/m) were used for AFM imaging under the following conditions: QI mode, 1.5 × 1.5 μm or 0.5 × 0.5 μm scan size, 128 × 128 pixels, Z-length 1 μm, setpoint 0.1 nN, and Z speed 166 μm/s. The Young's modulus was calculated using JPKSPM Data Processing software (Bruker). After averaging and baseline subtraction, Young's modulus was calculated using a Hertz model with a triangular pyramid half-cone angle of 35°.

SNP analysis. The genome data of *A. oryzae* required for SNP identification was obtained from the National Center for Biotechnology Information (NCBI). and mapped to *A. oryzae* RIB40 reference sequence using BWA-MEM2 (73). The SNPs were listed by FreeBayes (74), and detailed comparative analysis of genomes was performed on Integrative Genome Viewer (IGV) manually.

RNA seq. The RNA seq data have been deposited in DDBJ as BioProject PRJDB19992.

473

474 References

475 1. Amodeo, A. A. & Skotheim, J. M. Cell-Size Control. *Cold Spring Harb Perspect Biol* **8**,
476 a019083 (2016).
477 2. Nurse, P. Genetic control of cell size at cell division in yeast. *Nature* **256**, 547–551 (1975).
478 3. Jorgensen, P. *et al.* The Size of the Nucleus Increases as Yeast Cells Grow. *MBoC* **18**, 3523–
479 3532 (2007).
480 4. Dynesen J, Nielsen J. Branching is coordinated with mitosis in growing hyphae of *Aspergillus*
481 *nidulans*. *Fungal Genet Biol* 40, 15-24 (2003).
482 5. Dundon SE, Chang SS, Kumar A, Occhipinti P, Shroff H, Roper M, Gladfelter AS. Clustered
483 nuclei maintain autonomy and nucleocytoplasmic ratio control in a syncytium. *Mol Biol Cell*
484 **27**, 2000-7(2016).
485 6. Roper, M., Ellison, C., Taylor J. W. & Glass N. L. Nuclear and Genome Dynamics in
486 Multinucleate Ascomycete Fungi. *Curr Biol* **21**, R786-793 (2011).
487 7. Hurst, C. J. Microbial Fermentations in Nature and as Designed Processes. John Wiley & Sons
488 Ltd. (2023)
489 8. Kitamoto, K. Cell biology of the *Koji* mold *Aspergillus oryzae*. *Biosci, Biotechnol, Biochem* **79**,
490 863–869 (2015).
491 9. Ichishima, E. Development of enzyme technology for *Aspergillus oryzae*, *A. sojae*, and *A.*
492 *luchuensis,* the national microorganisms of Japan. *Bioscience, Biotechnology, and*
493 *Biochemistry* **80**, 1681–1692 (2016).
494 10. Yamashita, H. Koji Starter and Koji World in Japan. *JoF* **7**, 569 (2021).
495 11. Machida, M. *et al.* Genome sequencing and analysis of *Aspergillus oryzae*. *Nature* **438**, 1157–
496 1161 (2005).
497 12. Machida, M., Yamada, O. & Gomi, K. Genomics of Aspergillus oryzae: Learning from the
498 History of Koji Mold and Exploration of Its Future. *DNA Research* **15**, 173–183 (2008).
499 13. Gomi, K. Regulatory mechanisms for amylolytic gene expression in the koji mold *Aspergillus*
500 *oryzae*. *Bioscience, Biotechnology, and Biochemistry* **83**, 1385–1401 (2019).
501 14. Tanaka, M. & Gomi, K. Induction and Repression of Hydrolase Genes in *Aspergillus*
502 *oryzae*. *Front. Microbiol.* **12**, 677603 (2021).
503 15. Wang, B. *et al.* Survey of the transcriptome of *Aspergillus oryzae* via massively parallel mRNA
504 sequencing. *Nucleic Acids Research* **38**, 5075–5087 (2010).
505 16. Ishida, H. *et al.* Identification of functional elements that regulate the glucoamylase-encoding
506 gene (*glaB*) expressed in solid-state culture of *Aspergillus oryzae*. *Current Genetics* **37**, 373–
507 379 (2000).
508 17. Kitano, H., Kataoka, K., Furukawa, K. & Hara, S. Specific expression and temperature-

509 dependent expression of the acid protease-encoding gene (*pepA*) in *Aspergillus oryzae* in solid-
510 state culture (Rice-Koji). *J Biosci Bioengineering* **93**, 563–567 (2002).
511 18. Rokas, A. *et al.* What can comparative genomics tell us about species concepts in the genus
512 *Aspergillus*? *Studies in Mycology* **59**, 11–17 (2007).
513 19. Kusumoto, K.-I., Nogata, Y. & Ohta, H. Directed deletions in the aflatoxin biosynthesis gene
514 homolog cluster of *Aspergillus oryzae*. *Current Genetics* **37**, 104–111 (2000).
515 20. Kobayashi, T. *et al.* Genomics of *Aspergillus oryzae*. *Biosci, Biotechnol, Biochem* **71**, 646–670
516 (2007).
517 21. Watarai, N., Yamamoto, N., Sawada, K. & Yamada, T. Evolution of *Aspergillus oryzae* before
518 and after domestication inferred by large-scale comparative genomic analysis. *DNA Res* **26**,
519 465–472 (2019).
520 22. Chang, P.-K. & Ehrlich, K. C. What does genetic diversity of *Aspergillus flavus* tell us about
521 *Aspergillus oryzae*? *Internat J Food Microbiol* **138**, 189–199 (2010).
522 23. Gibbons, J. G. *et al.* The Evolutionary Imprint of Domestication on Genome Variation and
523 Function of the Filamentous Fungus *Aspergillus oryzae*. *Current Biol* **22**, 1403–1409 (2012).
524 24. Meyer, V. *et al.* Current challenges of research on filamentous fungi in relation to human
525 welfare and a sustainable bio-economy: a white paper. *Fungal Biol Biotechnol* **3**, 6, s40694-
526 016-0024–8 (2016).
527 25. Liu, D., Garrigues, S. & de Vries, R. P. Heterologous protein production in filamentous
528 fungi. *Appl Microbiol Biotechnol* **107**, 5019–5033 (2023).
529 26. Meyer, V. *et al.* Growing a circular economy with fungal biotechnology: a white paper. *Fungal*
530 *Biol Biotechnol* **7**, 5 (2020).
531 27. Christensen, T. *et al.* High Level Expression of Recombinant Genes in *Aspergillus oryzae. Nat*
532 *Biotechnol* **6**, 1419–1422 (1988).
533 28. Saito, N., Katayama, T., Minami, A., Oikawa, H. & Maruyama, J. Versatile filamentous fungal
534 host highly-producing heterologous natural products developed by genome editing-mediated
535 engineering of multiple metabolic pathways. *Commun Biol* **7**, 1263 (2024).
536 29. Huynh, H. H. *et al.* Functional production of human antibody by the filamentous fungus
537 *Aspergillus oryzae*. *Fungal Biol Biotechnol* **7**, 7 (2020).
538 30. Itoh, T., Tokunaga, K., Matsuda, Y. *et al.* Reconstitution of a fungal meroterpenoid biosynthesis
539 reveals the involvement of a novel family of terpene cyclases. *Nature Chem* **2**, 858–864 (2010).
540 31. Maini Rekdal, V., Villalobos-Escobedo, J.M., Rodriguez-Valeron, N. *et al. Neurospora*
541 *intermedia* from a traditional fermented food enables waste-to-food conversion. *Nat*
542 *Microbiol* **9**, 2666–2683 (2024).
543 32. Maini Rekdal, V., van der Luijt, C.R.B., Chen, Y. *et al.* Edible mycelium bioengineered for
544 enhanced nutritional value and sensory appeal using a modular synthetic biology toolkit. *Nat*

Commun **15**, 2099 (2024).

33. Yasui M, Oda K, Masuo S, Hosoda S, Katayama T, Maruyama JI, Takaya N, Takeshita N. Invasive growth of *Aspergillus oryzae* in rice koji and increase of nuclear number. *Fungal Biol Biotechnol*. 7, 8 (2020).
34. Hossain IM, Mazumder N, Kaino T, Kawamukai M, Noothalapati H, Yamamoto T. Direct Visualization of Structurally Similar Polysaccharides in Single Yeast Cells in Vivo by Multivariate Analysis Assisted Raman Microspectroscopy. *J Phys Chem B* 127, 5249-5256 (2023).
35. Yasuda, M., Takeshita, N. & Shigeto, S. Inhomogeneous Molecular Distributions and Cytochrome Types and Redox States in Fungal Cells Revealed by Raman Hyperspectral Imaging Using Multivariate Curve Resolution–Alternating Least Squares. *Anal. Chem.* **91**, 12501–12508 (2019).
36. Itani, A., Shida, Y. & Ogasawara, W. A microfluidic device for simultaneous detection of enzyme secretion and elongation of a single hypha. *Front. Microbiol.* **14**, 1125760 (2023).
37. Wouters, B. G. & Koritzinsky, M. Hypoxia signalling through mTOR and the unfolded protein response in cancer. *Nat Rev Cancer* **8**, 851–864 (2008).
38. Nakayama, Y., Yoshimura, K. & Iida, H. Organellar mechanosensitive channels in fission yeast regulate the hypo-osmotic shock response. *Nat Commun* **3**, 1020 (2012).
39. Nakayama, Y., Hirata, A. & Iida, H. Mechanosensitive channels Msy1 and Msy2 are required for maintaining organelle integrity upon hypoosmotic shock in *Schizosaccharomyces pombe*. *FEMS Yeast Res* **14**, 992–994 (2014).
40. Ogawa, M. *et al.* Deletion of *Aspergillus nidulans cpsA/rseA* induces increased extracellular hydrolase production in solid-state culture partly through the high osmolarity glycerol pathway. *J Biosci Bioeng* **131**, 589–598 (2021).
41. Vitikainen, M. *et al.* Array comparative genomic hybridization analysis of Trichoderma reesei strains with enhanced cellulase production properties. *BMC Genomics* **11**, 441 (2010).
42. Barreiro, C., Martín, J. F. & García-Estrada, C. Proteomics Shows New Faces for the Old Penicillin Producer *Penicillium chrysogenum*. *J Biomed Biotechnol* **2012**, 1–15 (2012).
43. Murphy, C. M. & Michael, W. M. Control of DNA Replication by the Nucleus/Cytoplasm Ratio in Xenopus. *J Biol Chem* **288**, 29382–29393 (2013).
44. Futcher, B. & Kellogg, D. R. SnapShot: Cell size control. *Cell* **187**, 2896-2896.e1 (2024).
45. Fantes, P. & Nurse, P. Control of cell size at division in fission yeast by a growth-modulated size control over nuclear division. *Experiment Cell Research* **107**, 377–386 (1977).
46. Bergen, L. G. & Morris, N. R. Kinetics of the nuclear division cycle of *Aspergillus nidulans*. *J Bacteriol* **156**, 155–160 (1983).
47. Dörter, I. & Momany, M. Fungal Cell Cycle: A Unicellular versus Multicellular

581 Comparison. *Microbiol Spectr* **4**, 4.6.28 (2016).
582 48. Gould, K. L. & Nurse, P. Tyrosine phosphorylation of the fission yeast cdc2+ protein kinase
583 regulates entry into mitosis. *Nature* **342**, 39–45 (1989).
584 49. Wu, L., Osmani, S. A. & Mirabito, P. M. A Role for NIMA in the Nuclear Localization of
585 Cyclin B in *Aspergillus nidulans*. *J Cell Biol* **141**, 1575–1587 (1998).
586 50. Ye, X. S., Fincher, R. R., Tang, A. & Osmani, S. A. The G2/M DNA damage checkpoint
587 inhibits mitosis through Tyr15 phosphorylation of p34cdc2 in *Aspergillus nidulans*. *EMBO*
588 *J* **16**, 182–192 (1997).
589 51. Shen, K. F. & Osmani, S. A. Regulation of mitosis by the NIMA kinase involves TINA and its
590 newly discovered partner, An-WDR8, at spindle pole bodies. *MBoC* **24**, 3842–3856 (2013).
591 52. Osmani, S. A., May, G. S. & Morris, N. R. Regulation of the mRNA levels of *nimA*, a gene
592 required for the G2-M transition in *Aspergillus nidulans*. *J Cell Biol* **104**, 1495–1504 (1987).
593 53. Osmani, A. H., O'Donnell, K., Pu, R. T. & Osmani, S. A. Activation of the *nimA* protein kinase
594 plays a unique role during mitosis that cannot be bypassed by absence of the *bimE* checkpoint.
595 *EMBO J* **10**, 2669–2679 (1991).
596 54. Harris, S.D. Branching of fungal hyphae: regulation, mechanisms and comparison with other
597 branching systems. *Mycologia* **100**, 823-32 (2008).
598 55. Feng, X. *et al. cpsA* regulates mycotoxin production, morphogenesis and cell wall biosynthesis
599 in the fungus *Aspergillus nidulans*. *Mol Microbiol* **105**, 1–24 (2017).
600 56. Urban, J. *et al.* Sch9 Is a Major Target of TORC1 in *Saccharomyces cerevisiae*. *Molecular*
601 *Cell* **26**, 663–674 (2007).
602 57. De Virgilio, C. & Loewith, R. The TOR signalling network from yeast to man. *The Internat J*
603 *Biochem Cell Biol* **38**, 1476–1481 (2006).
604 58. Kim, J. & Guan, K.-L. mTOR as a central hub of nutrient signalling and cell growth. *Nat Cell*
605 *Biol* **21**, 63–71 (2019).
606 59. Saxton, R. A. & Sabatini, D. M. mTOR Signaling in Growth, Metabolism, and
607 Disease. *Cell* **169**, 361–371 (2017).
608 60. Meng, D. *et al.* Glutamine and asparagine activate mTORC1 independently of Rag GTPases. *J*
609 *Biol Chem* **295**, 2890–2899 (2020).
610 61. Düvel, K. *et al.* Activation of a Metabolic Gene Regulatory Network Downstream of mTOR
611 Complex 1. *Mol Cell* **39**, 171–183 (2010).
612 62. Clutterbuck, A.J. Synchronous Nuclear Division and Septation in *Aspergillus nidulans. J Gen*
613 *Microbiol* **60**, 133-135 (1970).
614 63. Vinck, A., Terlou, M., Pestman, W.R., Martens, E.P., Ram, A.F., van den Hondel, C.A., Wösten,
615 H.A. Hyphal differentiation in the exploring mycelium of *Aspergillus niger. Mol Microbiol* **58**,
616 693-9 (2005).

64. Wada, R., Maruyama, J., Yamaguchi, H., Yamamoto, N., Wagu, Y., Paoletti, M., Archer, D.B., Dyer, P.S., Kitamoto, K. Presence and functionality of mating type genes in the supposedly asexual filamentous fungus *Aspergillus oryzae. Appl Environ Microbiol* **78**, 2819-29 (2012).
65. Lee, B.N., Adams, T.H. Overexpression of *flbA*, an early regulator of *Aspergillus* asexual sporulation, leads to activation of *brlA* and premature initiation of development. *Mol Microbiol* **14**, 323-34 (1994).
66. Roper, M., Ellison, C., Taylor J. W. & Glass N. L. Nuclear and Genome Dynamics in Multinucleate Ascomycete Fungi. *Curr Biol* **21**, R786-793 (2011).
67. Havlik, D., Brandt, U., Bohle, K. & Fleißner, A. Establishment of *Neurospora crassa* as a host for heterologous protein production using a human antibody fragment as a model product. *Microbial Cell Factories* **16**, 128 (2017).
68. Jacobson, D. J. et al. *Neurospora* in temperate forests of western North America. *Mycologia* **96**, 66–74 (2004).
69. Kokkoris V, Stefani F, Dalpé Y, Dettman J, Corradi N. Nuclear Dynamics in the Arbuscular Mycorrhizal Fungi. *Trends Plant Sci.* **25**, 765-778 (2020).
70. Katayama, T. *et al.* Forced Recycling of an AMA1-Based Genome-Editing Plasmid Allows for Efficient Multiple Gene Deletion/Integration in the Industrial Filamentous Fungus *Aspergillus oryzae*. *Appl Environ Microbiol* **85**, e01896-18 (2019).
71. Ge, S. X., Jung, D. & Yao, R. ShinyGO: a graphical gene-set enrichment tool for animals and plants. *Bioinformatics* **36**, 2628–2629 (2020).
72. Waskom, M. seaborn: statistical data visualization. *JOSS* **6**, 3021 (2021).
73. Vasimuddin, M., Misra, S., Li, H. & Aluru, S. Efficient Architecture-Aware Acceleration of BWA-MEM for Multicore Systems. *IEEE Parallel and Distributed Processing Symposium (IPDPS)*, 314-324 (2019)
74. Garrison, E. & Marth, G. Haplotype-based variant detection from short-read sequencing. arXiv:1207.3907 [q-bio.GN] https://doi.org/10.48550/arXiv.1207.3907

647 **Figure legends.**

648 Figure 1. Increase in number of nuclei and cell volume in *Aspergillus* species. (A) The nuclear
649 distribution in the tip cells was categorized into Classes I–III. The ratio of hyphae in each class was
650 measured in *Aspergillus* species at 24, 48, and 72 hours of growth (n=50). Data for *A. oryzae* RIB40
651 and *A. nidulans* are reproduced from a previous study (33). (B) Colony morphology after 3 days of
652 culture on the minimal medium. The nuclear distribution in the hyphae at the colony periphery stained
653 with SYBR Green. Scale bars: hyphae, 20 μm; colonies, 1 cm. (C) 3D images of hyphae without
654 increased nuclei (left) and with increased nuclei (right) in *A. oryzae* RIB40 from Movie 1. Each
655 nucleus is indicated with different colors by Imaris soft. Scale bar: 5 μm. (D) Comparison of nuclear
656 size in Class I hyphae (2.4 μm) and Class III hyphae (1.6 μm), indicated by white lines. (E) Box plots
657 of nucleus diameters in hyphae without increased nuclei and those with increased nuclei (n=35, ** p
658 < 0.01, t-test). (F) Box plots of hyphal width at the colony periphery grown for 72 hours (n=10–14, **
659 p< 0.01, * p< 0.05, t-test). Strains with increased nuclei are marked in red, and those without are
660 marked in blue. (G) Correlation between nuclear number and cell volume of hyphae at 100 μm from
661 the tips in *A. oryzae* RIB40, RIB128, RIB915, and *A. flavus*.

662

663 Figure 2. Thick hyphae with increased nuclei emerge by branching. (A) Time-lapse image sequence
664 of *A. oryzae* RIB40 expressing H2B-GFP showing the emergence of thick hyphae with increased
665 nuclei by branching from Movie 2. Scale bar: 20 μm. Elapsed time is indicated in min. (B) Image
666 sequence of successive nuclear division within the newly emerged branched hypha from Movie 3.
667 Scale bar: 10 μm. Elapsed time is indicated in min. (C) Time course of nuclear number per hypha.
668 Nuclear numbers were counted with the start time of branching set as 0, every hour for 5 to 10 h.
669 Thick; hyphal width >7 μm, Thin; hyphal width <5 μm. (D) Branching from hyphae with increased
670 nuclei generates both thick hyphae with increased nuclei (left) and thin hyphae without increased

671 nuclei (right). Scale bars: 20 μm. (E) Image sequence of mycelial growth showing hyphae with
672 increased nuclei (green) and without increased nuclei (white) from Movie 4. Scale bars: 200 μm.
673 Elapsed time is indicated in h. (F) Line histogram of hyphal width at the colony periphery at 20, 40,
674 and 60 h, calculated from Movie 4 (n=40). (G) Correlation between hyphal width and maximum
675 elongation rate calculated from Movie 4 (n=45). The maximum elongation rate is determined from
676 elongation rates measured every hour over 10 hours period. (H) TEM images of *A. oryzae* RIB40
677 hyphae. Hyphal diameter and cell wall thickness are indicated white and black text respectively. Scale
678 bar: 1 μm. (I) Correlation plots of hyphal width and cell wall thickness based on TEM images. Thick
679 hyphae (>7 μm) are marked in red, and thin hyphae (<7 μm) are marked in blue. (J) 3D surface images
680 of *A. oryzae* RIB40 hyphal tips in the thick hypha (upper) and the thin hypha (lower) constructed using
681 AFM. (K) Surface roughness of cell walls in thick (red) and thin (blue) hyphae along the arrows in J.
682
683 Figure 3. Correlation between number of nuclei and enzyme secretion. (A) Secreted protein per
684 biomass in strains with increased nuclei (red) and without increased nuclei (blue) after 4 days of culture
685 in minimal medium with 1% maltose (mean ± S.E., n=3, ** $p < 0.01$, t-test). (B) Time course of α-
686 amylase activity per biomass in *A. oryzae* RIB40 and RIB915 cultured in minimal medium with 1%
687 maltose (mean ± S.E., n=3). (C) Measurement of α-amylase activity in a single hypha using a
688 microfluidic device. A fluorescent substrate increases in fluorescence upon hydrolysis by α-amylase.
689 ROIs for thick hypha are marked in red, and thin hypha in blue. Scale bar: 10 μm. (D) Temporal
690 changes in fluorescence intensity measured in individual flow channels, as described in C. (E) Box
691 plots of hyphal width in colonies grown in minimal medium with or without 1% yeast extract (n=10–
692 18, ** $p < 0.01$, * $p < 0.05$, t-test). Conditions with increased nuclei are marked in red, and those
693 without in blue. (F) Secreted protein per biomass in minimal medium with or without 1% yeast extract
694 (mean ± S.E., n=3, ** $p < 0.01$, t-test). (G) Ratio of class I-III hyphae in *A. oryzae* RIB915 colonies

695 grown in minimal medium supplemented with 1% yeast extract or 0.1% individual amino acids (n=50).
696 (H) Correlation between the ratio of Class III hyphae and secreted protein per biomass in the 0.1%
697 amino acid-supplemented medium. (I) Images of hyphae and nuclear distribution in *A. oryzae* RIB40
698 grown on minimal medium with or without 0.5 ng/ml rapamycin. Scale bars: 10 μm. (J) Ratio of class
699 I-III hyphae in *A. oryzae* RIB40 cultured on minimal medium containing 0, 0.5, 5, or 100 ng/ml
700 rapamycin (n=50). (K) Box plots of hyphal width in the colonies cultured under the conditions in J
701 (n=11-18, ** $p < 0.01$, t-test).
702
703 Figure 4. Transcriptome analyses in hyphae with increased nuclei. (A) Heatmap of gene expression in
704 *A. oryzae* RIB40, RIB915, and *A. nidulans* grown in the minimal medium with or without 1% yeast
705 extract. The top 500 genes with the largest variation in expression are shown. (B) Venn diagram of
706 genes upregulated more than four-fold in the medium with yeast extract. (C) GO process analysis of
707 genes uniquely upregulated in *A. oryzae* RIB915 grown in the medium with yeast extract. (D) Image
708 sequence of cutting and collecting the targeted hypha by using laser microdissection. Scale bar: 100
709 μm. (E) Heatmap of gene expression in thick (n=3) and thin (n=2) hyphae dissected from *A. oryzae*
710 RIB40. The top 300 genes with the largest expression differences are shown. (F) GO process analysis
711 of genes upregulated more than four-fold in thick hyphae compared to thin hyphae. (G) Venn diagram
712 of 449 genes upregulated in RIB915 with yeast extract and 558 genes upregulated in thick hyphae of
713 RIB40. (H) GO annotations of 13 genes from the 21 shared genes in G. Genes related to cell wall
714 processes are shown in green, cell membrane in blue, Ca^{2+} transport in yellow, and rRNA processing
715 in orange. (I) Images of hyphae of RIB40 and Δ*msyA* strains after 3 min of low osmotic stress. Scale
716 bar: 200 μm. (J) Ratio of hyphal tip lysis under the hypoosmotic shock (mean ± S.E., n=50, ** $p <$
717 0.01, t-test).
718

719 Figure 5. Comparison of industrial bred strains in *A. oryzae, T. reesei* and *P. chrysogenum*. (A)
720 Phylogenetic clade A-F of *A. oryzae* TK strains. The strains with increased nuclei are indicated in red.
721 (B) Colonies and hyphae stained with SYBR Green of strains in clades C, F, and G grown for 3 days
722 on the minimal medium. Scale bar: 20 μm. (C) Sequence differences in *rseA* gene among strains in
723 clades C, F, and G. UTR regions are marked in pink, exons in purple, and nucleotide differences in
724 white. (D) Colonies and hyphae stained with SYBR Green of RIB40 and the Δ*rseA* strain grown for 3
725 days on the minimal medium. Scale bar: 10 μm. (E) Colonies and hyphae stained with SYBR Green
726 of RIB915 expressing *rseA* gene from RIB40 and TK-47 strains with increased nuclei, and TK-41
727 strain without increased nuclei. Scale bar: 20 μm. (F) Hyphal width of RIB915 and strains in E (n=14–
728 23). Strains with *rseA* from strains with increased nuclei are marked in red, and those without are
729 marked in blue. (G) Hyphal images stained with SYBR Green of *T. reesei* (QM9414) and *P.*
730 *chrysogenum* (IFO4688) grown for 3 days on the minimal medium with or without 1% yeast extract.
731 Scale bar: 20 μm. (H) Ratio of class I-III hyphae in the *T. reesei* and *P. chrysogenum* control and bred
732 strains cultured on the minimal medium with or without 1% yeast extract for 3 days (n=50). (I)
733 CMCase activity per biomass of *T. reesei* industrial and control strains under the conditions in G (mean
734 ± S.E., n=3, ** $p < 0.01$, t-test). (J) Protease activity per biomass of *P. chrysogenum* industrial and
735 control strains under the conditions in G (mean ± S.E., n=3, ** $p < 0.01$, t-test).
736
737 Figure 6. (A) Molecular mechanism by which cell volume and nucelar number regulate each other and
738 each increases simultaneously. (B) An increase in the number of nuclei per hyphal cell enhances
739 transcription, translation, and enzyme secretion per cell.
740

Fig. 1

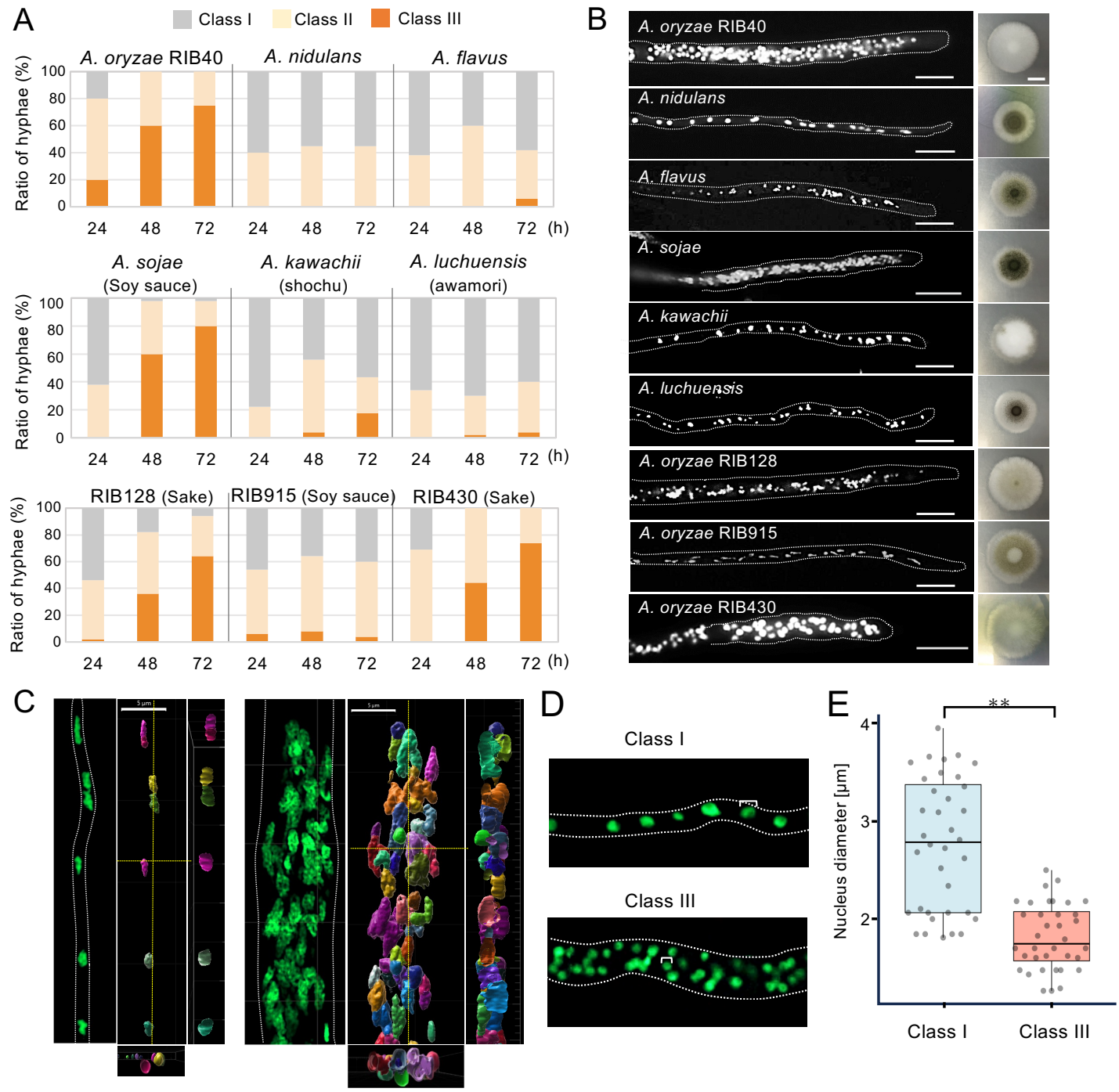
A
Class I
Class II
Class III
A. oryzae RIB40
A. nidulans
A. flavus
A. sojae (Soy sauce)
A. kawachii (shochu)
A. luchuensis (awamori)
RIB128 (Sake)
RIB915 (Soy sauce)
RIB430 (Sake)
Ratio of hyphae (%)
(h)
B
A. oryzae RIB40
A. nidulans
A. flavus
A. sojae
A. kawachii
A. luchuensis
A. oryzae RIB128
A. oryzae RIB915
A. oryzae RIB430
C
D
Class I
Class III
E
Nucleus diameter [μm]
Class I
Class III
F
Hyphal width [μm]
ns
RIB40
RIB128
RIB915
A. sojae
A. nidulans
A. flavus
A. kawachii
A. luchuensis
A. oryzae
G
RIB40
RIB128
RIB915
A. flavus
R² = 0.94
Number of nuclei
Cell volume [×10³ μm³]

Fig. 2

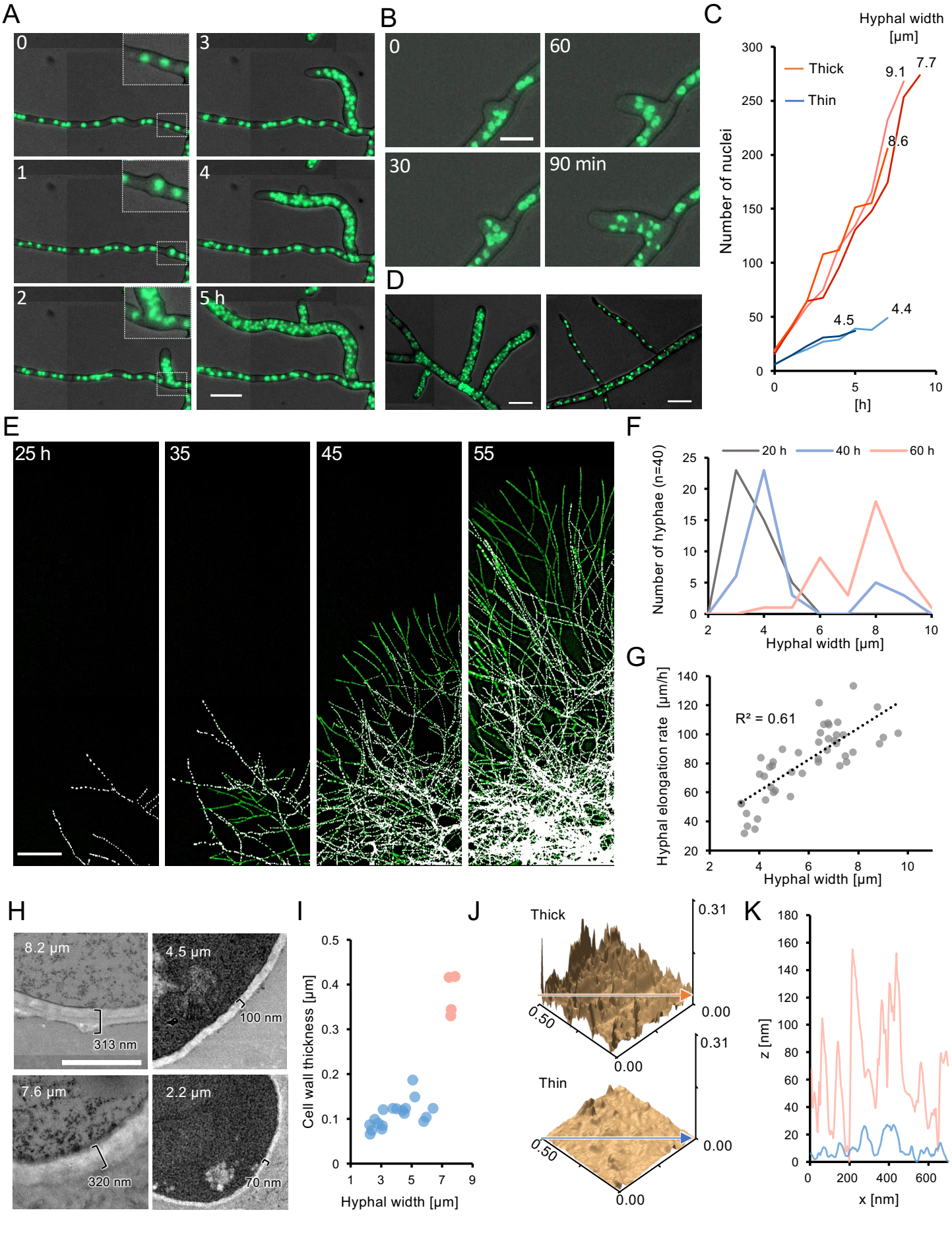
A
0
3
1
4
2
5 h
B
0
60
30
90 min
C
Hyphal width [µm]
Thick
Thin
9.1
7.7
8.6
4.5
4.4
Number of nuclei
[h]
D
E
25 h
35
45
55
F
20 h
40 h
60 h
Number of hyphae (n=40)
Hyphal width [µm]
G
R² = 0.61
Hyphal elongation rate [µm/h]
Hyphal width [µm]
H
8.2 µm
313 nm
4.5 µm
100 nm
7.6 µm
320 nm
2.2 µm
70 nm
I
Cell wall thickness [µm]
Hyphal width [µm]
J
Thick
Thin
0.31
0.00
0.50
0.00
K
z [nm]
x [nm]

Fig. 3

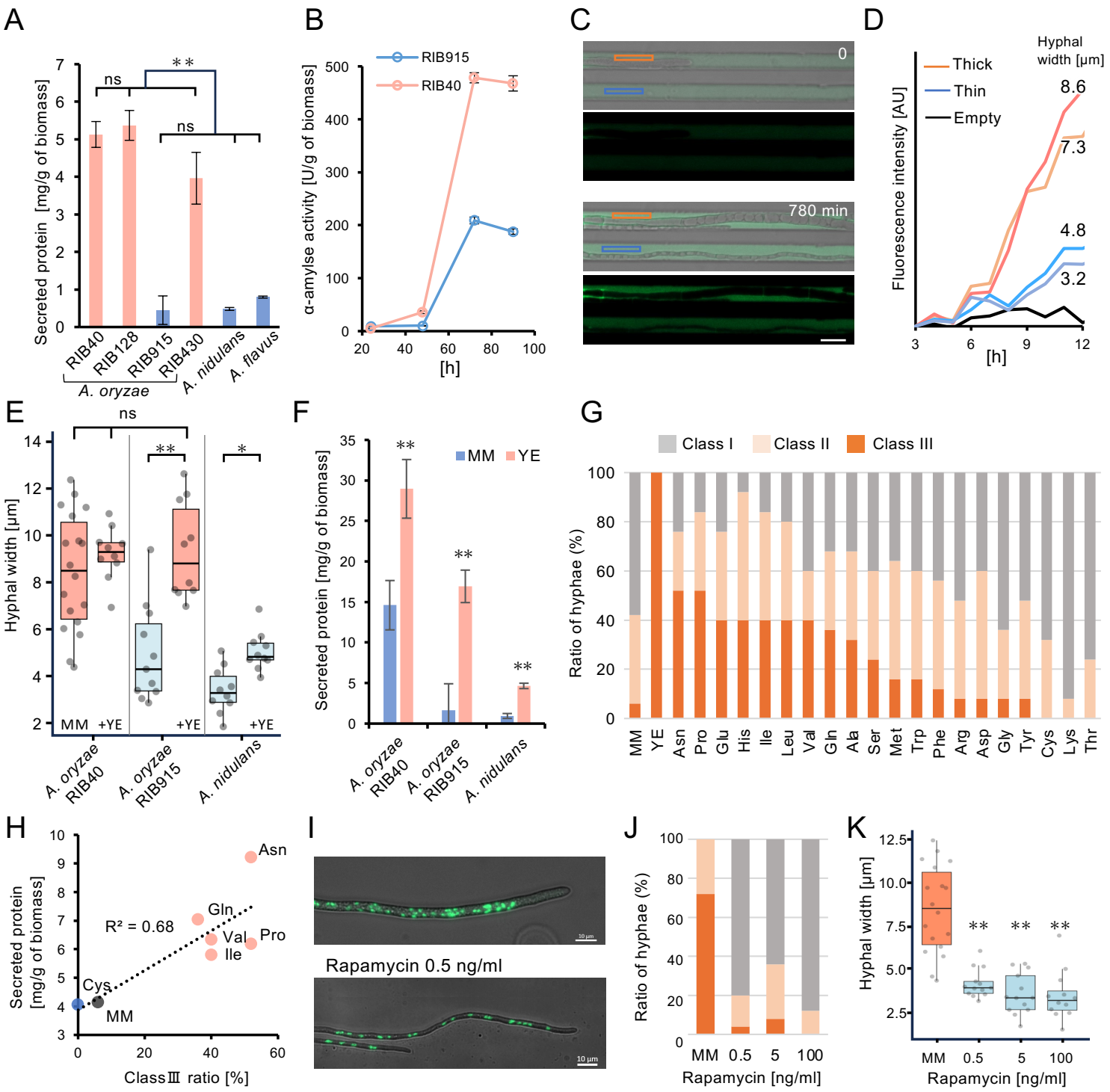
A
Secreted protein [mg/g of biomass]
ns
**
ns
RIB40
RIB128
RIB915
RIB430
A. nidulans
A. flavus
A. oryzae
B
α-amylse activity [U/g of biomass]
RIB915
RIB40
[h]
C
0
780 min
D
Hyphal width [μm]
Thick
Thin
Empty
8.6
7.3
4.8
3.2
Fluorescence intensity [AU]
[h]
E
Hyphal width [μm]
ns
**
*
MM
+YE
+YE
+YE
A. oryzae RIB40
A. oryzae RIB915
A. nidulans
F
Secreted protein [mg/g of biomass]
MM
YE
**
**
**
A. oryzae RIB40
A. oryzae RIB915
A. nidulans
G
Class I
Class II
Class III
Ratio of hyphae (%)
MM
YE
Asn
Pro
Glu
His
Ile
Leu
Val
Gln
Ala
Ser
Met
Trp
Phe
Arg
Asp
Gly
Tyr
Cys
Lys
Thr
H
Secreted protein [mg/g of biomass]
Asn
Gln
R² = 0.68
Val
Pro
Ile
Cys
MM
ClassⅢ ratio [%]
I
Rapamycin 0.5 ng/ml
10 μm
10 μm
J
Ratio of hyphae (%)
MM
0.5
5
100
Rapamycin [ng/ml]
K
Hyphal width [μm]
**
**
**
MM
0.5
5
100
Rapamycin [ng/ml]

Fig. 4

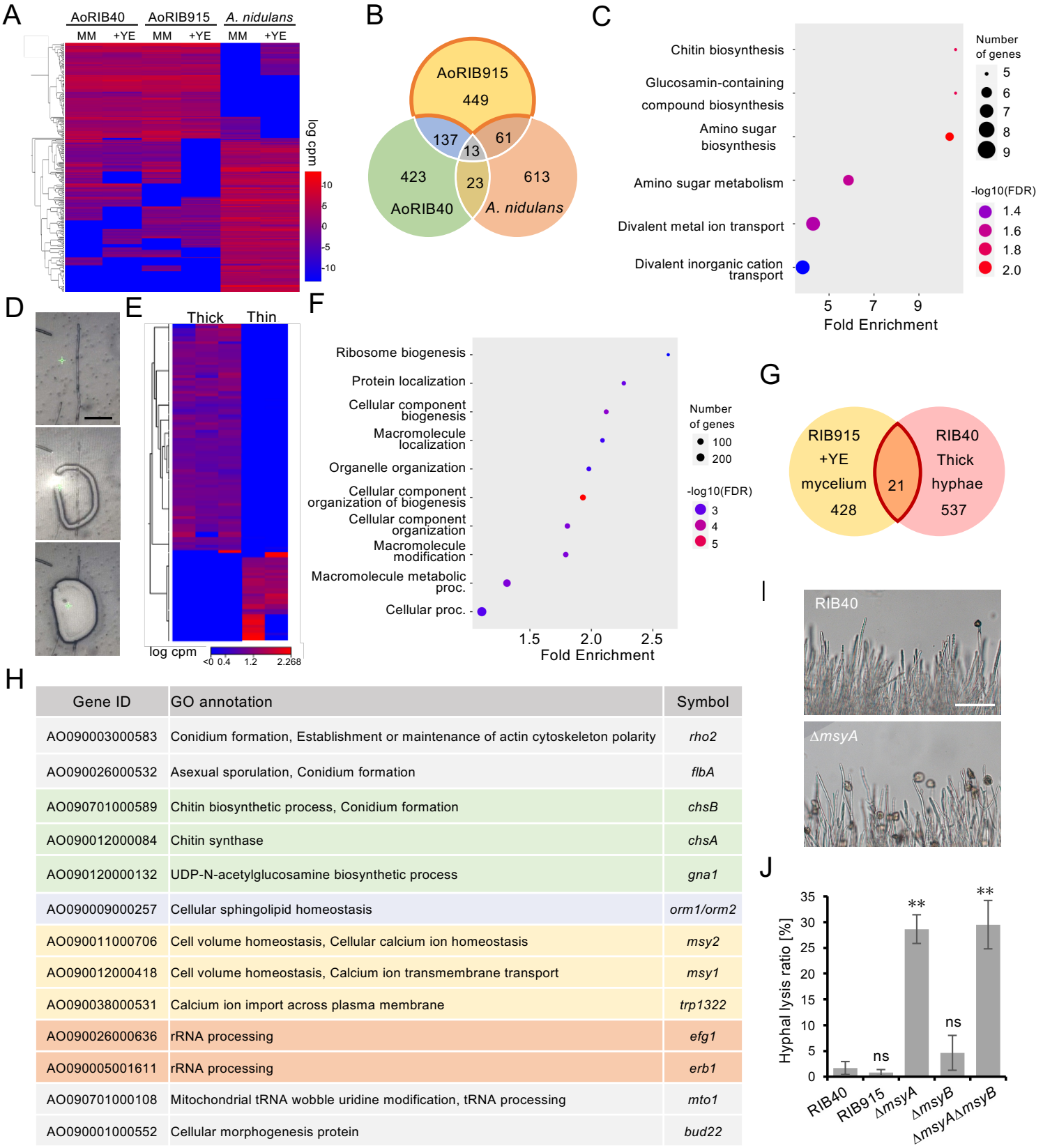

H

Gene ID	GO annotation	Symbol
AO090003000583	Conidium formation, Establishment or maintenance of actin cytoskeleton polarity	*rho2*
AO090026000532	Asexual sporulation, Conidium formation	*flbA*
AO090701000589	Chitin biosynthetic process, Conidium formation	*chsB*
AO090012000084	Chitin synthase	*chsA*
AO090120000132	UDP-N-acetylglucosamine biosynthetic process	*gna1*
AO090009000257	Cellular sphingolipid homeostasis	*orm1/orm2*
AO090011000706	Cell volume homeostasis, Cellular calcium ion homeostasis	*msy2*
AO090012000418	Cell volume homeostasis, Calcium ion transmembrane transport	*msy1*
AO090038000531	Calcium ion import across plasma membrane	*trp1322*
AO090026000636	rRNA processing	*efg1*
AO090005001611	rRNA processing	*erb1*
AO090701000108	Mitochondrial tRNA wobble uridine modification, tRNA processing	*mto1*
AO090001000552	Cellular morphogenesis protein	*bud22*

Fig. 5

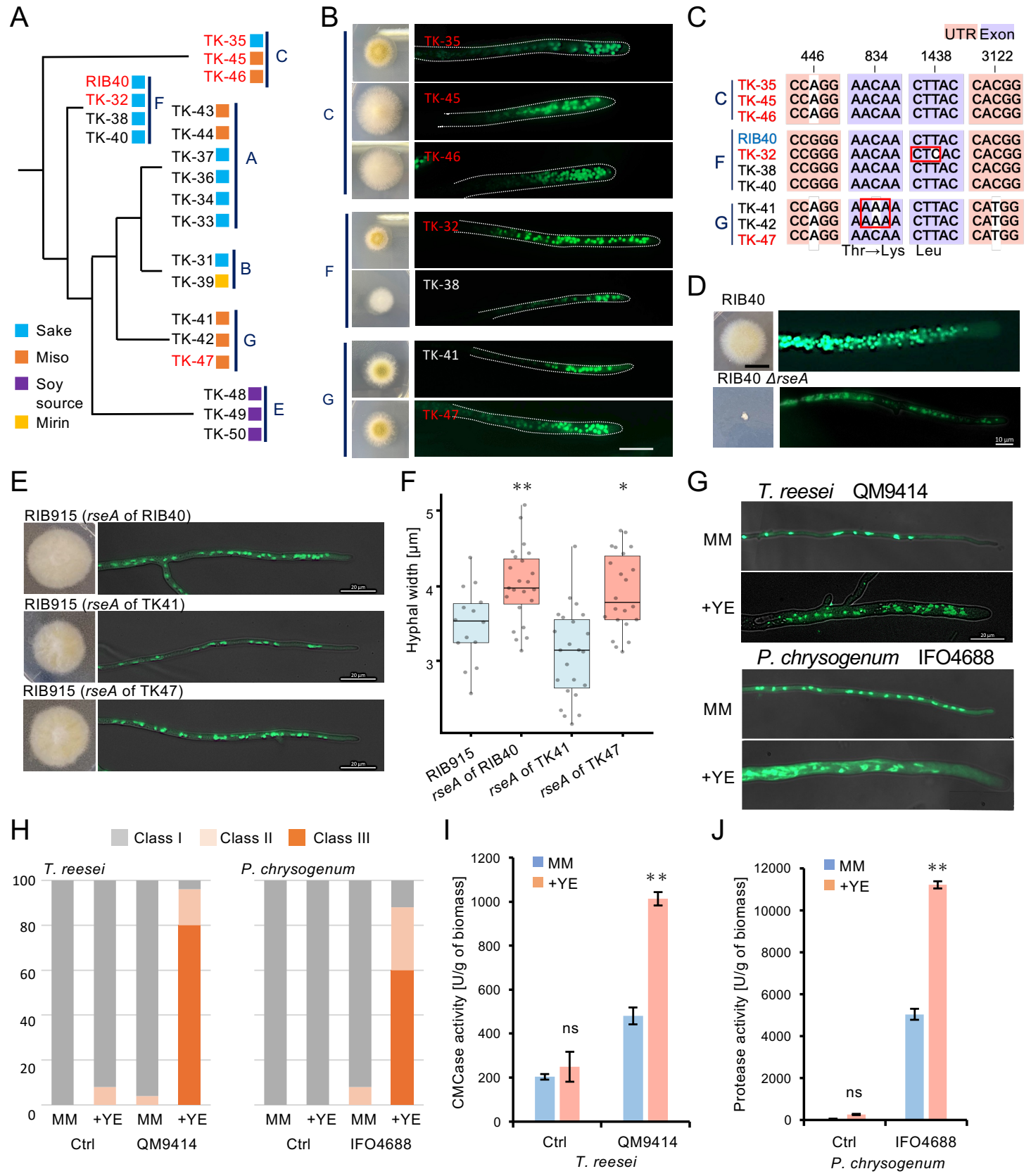
A
TK-35
TK-45
TK-46
C
RIB40
TK-32
TK-38
TK-40
F
TK-43
TK-44
TK-37
TK-36
TK-34
TK-33
A
TK-31
TK-39
B
TK-41
TK-42
TK-47
G
TK-48
TK-49
TK-50
E
Sake
Miso
Soy source
Mirin
B
C
TK-35
TK-45
TK-46
F
TK-32
TK-38
G
TK-41
TK-47
C
UTR Exon
446 834 1438 3122
C TK-35 CCAGG AACAA CTTAC CACGG
TK-45 CCAGG AACAA CTTAC CACGG
TK-46 CCAGG AACAA CTTAC CACGG
F RIB40 CCGGG AACAA CTTAC CACGG
TK-32 CCGGG AACAA CTCAC CACGG
TK-38 CCGGG AACAA CTTAC CACGG
TK-40 CCGGG AACAA CTTAC CACGG
G TK-41 CCAGG AAAAA CTTAC CATGG
TK-42 CCAGG AAAAA CTTAC CATGG
TK-47 CCAGG AACAA CTTAC CATGG
Thr→Lys Leu
D
RIB40
RIB40 ΔrseA
10 μm
E
RIB915 (rseA of RIB40)
RIB915 (rseA of TK41)
RIB915 (rseA of TK47)
20 μm
F
Hyphal width [μm]
5
4
3
**
*
RIB915
rseA of RIB40
rseA of TK41
rseA of TK47
G
T. reesei QM9414
MM
+YE
P. chrysogenum IFO4688
MM
+YE
20 μm
H
Class I
Class II
Class III
T. reesei
P. chrysogenum
100
80
60
40
20
0
MM +YE MM +YE
Ctrl QM9414
MM +YE MM +YE
Ctrl IFO4688
I
MM
+YE
CMCase activity [U/g of biomass]
1200
1000
800
600
400
200
0
ns
**
Ctrl QM9414
T. reesei
J
MM
+YE
Protease activity [U/g of biomass]
12000
10000
8000
6000
4000
2000
0
ns
**
Ctrl IFO4688
P. chrysogenum

Fig. 6

A

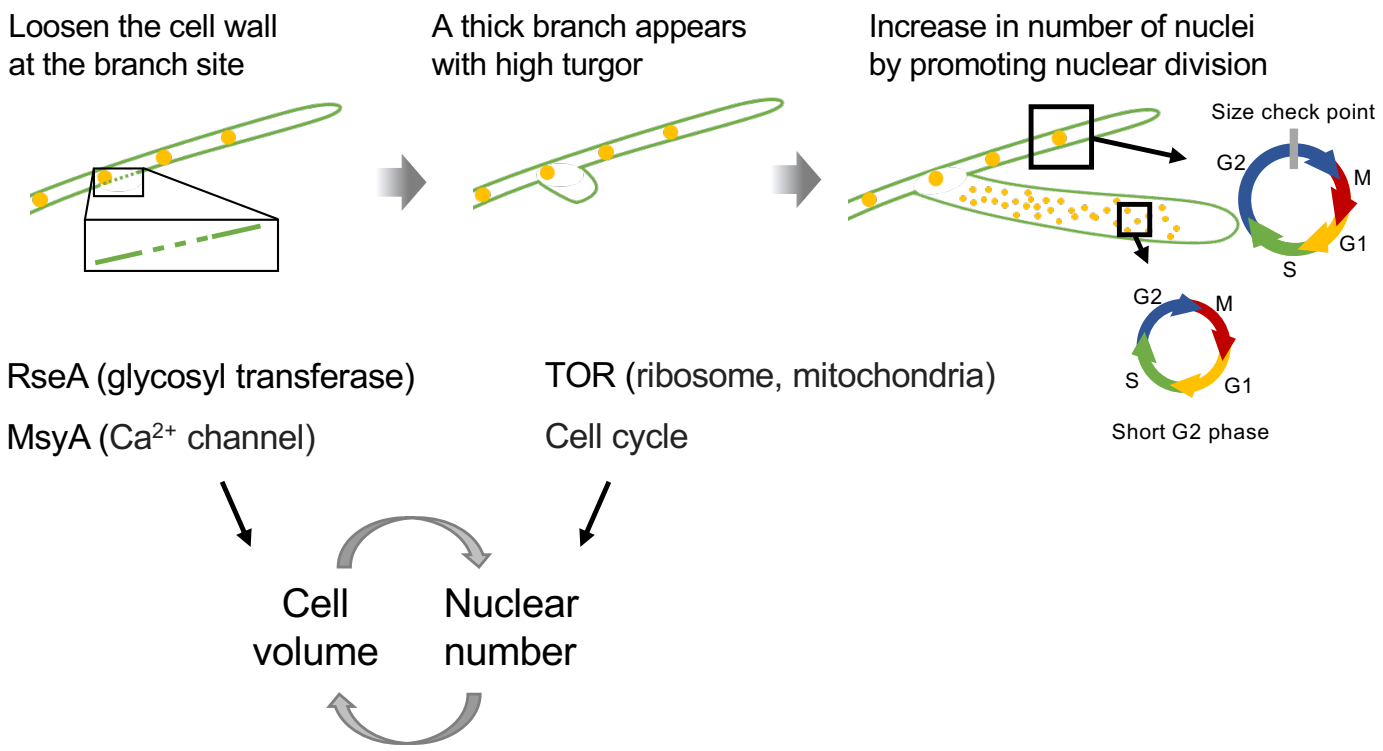
Loosen the cell wall
at the branch site
A thick branch appears
with high turgor
Increase in number of nuclei
by promoting nuclear division
Size check point
G2
M
G1
S
G2
M
S
G1
Short G2 phase
RseA (glycosyl transferase)
MsyA (Ca2+ channel)
TOR (ribosome, mitochondria)
Cell cycle
Cell
volume
Nuclear
number
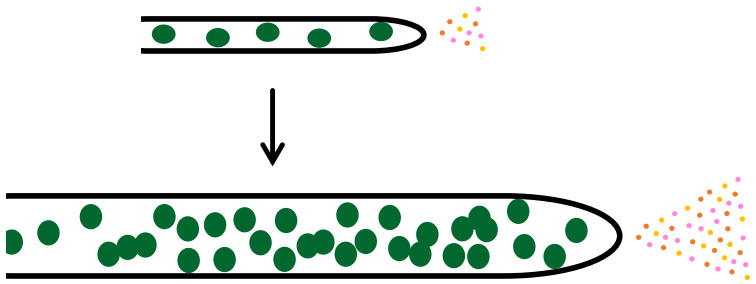
B